CHAPTER IV
POLYETHYLENIMINE CONTAINING BENZIMIDAZOLE BRANCHING: A MODEL SYSTEM PROVIDING A BALANCE OF HYDROGEN BOND NETWORK OR CHAIN MOBILITY ENHANCES PROTON CONDUCTIVITY

4.1 Abstract

A series of multi-benzimidazole functionalized branched polyethylenimine (MPEI) with varied benzimidazole substitution are designed and synthesized to study how hydrogen bonds of benzimidazole can be enhanced through the branching structure of polymer chains. The reduction of H-bonding and the increment of inter-atomic distance distribution initiate an increase in proton conductivity with temperature as detailed analyses by temperature dependence Fourier transform infrared (FTIR) spectroscopy and radial distribution function calculated from temperature dependence X-ray diffraction technique. MPEIs with the higher benzimidazole substitution perform the more number of hydrogen bonds together with the lowering of chain mobility. Combining with the proton conductivity evaluation, *b*PEI with 19.7 % benzimidazole substitution is a preferable condition since at this condition both hydrogen bond and chain mobility are in good balance favor the proton transfer resulting in a significant proton conductivity ~10^{-5} S cm^{-1} in the case of pure sample in pellet form and ~10^{-4} S cm^{-1} in the case of the blend with PVA in membrane form measuring at 190 °C under anhydrous condition.

Keywords: Polymer electrolyte membrane; Hydrogen bonding; Benzimidazole; Branched polyethylenimine, Proton transfer

4.2 Introduction

Polymer electrolyte membrane fuel cell (PEMFC) has been developed to become one of the most promising clean power generation technologies for vehicles and portable devices.[1-3] Polymer electrolyte membrane (PEM) is a key component

performing proton conduction in PEMFC. At present, perfluorosulfonic acid polymer e.g., Nafion®, is considered as the most practical electrolyte membrane due to its excellent proton conductivity as well as its high thermal and chemical stabilities.[4,5] However, some drawbacks of Nafion®, for example, the high cost and the low working temperature range (lower than 100 °C),[6-8] lead to an expectation of alternative materials for the use in high temperature PEMFC (100-200 °C).

Nitrogen containing heterocyclic based structures e.g., imidazole, pyrazole, and benzimidazole are proposed as high thermally stable proton conductive molecules.[9-11] The proton transfer mechanism of the heterocycles occurs basically through protonation of the resonance structure followed by proton transfer and reorientation under hydrogen bond network.[12] Various types of heterocycle based PEMs such as homo- and copolymer of heterocycles,[11,13-15] linear polymers grafted with heterocycles,[16-19] and polymer blends with heterocycles[20-22] have been reported. Their proton conductivities were found to be related to several factors. For instance, Kreuer et al. found that imidazole and pyrazole form hydrogen bond network for acidic proton in polymer transport.[9] The increment of imidazole and pyrazole intercalated into sulfonated polyetherketone enhances proton conductivity. Higher tendency to form hydrogen bond of imidazole results in higher proton conductivity compared with the case of pyrazole. Moreover, poly(acrylic acid) entrapped with imidazole[23] and poly(4(5)-vinylimidazole-*co*-ethyleneglycol methacrylate phosphate[24] were also reported to find the increase of proton conductivity with an increase of imidazole units. Persson et al. developed benzimidazole tethered on linear polysiloxane[16] and poly(ethylene oxide)[18] and showed the conductivity for 10^{-6} S cm^{-1}. It is important to note that those reports showed us that the proton conductivities were not only depending on the benzimidazole concentrations but also segmental mobility of the polymer chains.

Polyethylenimine (PEI) is a commercially available polymer in linear and branch forms. Linear PEI (*l*PEI) consists of secondary amine species along the polymer chain and primary amine species at the terminal chain ends whereas branched PEI (*b*PEI) consists of primary, secondary and tertiary amine species in random manner. Due to reactive amines in the structure, modifications of PEIs with numerous functional groups, for example, with palmitic acid, ethyl acrylate,

polyamide, and poly(ethylene glycol), etc, were reported.[25-27] Recently, Yang et al. proposed nanocomposite membrane of trifluoromethanesulfonimide doped /PEI/SiO_2 for the use in PEMFC at high temperature with the proton conductivity as high as $5.6x10^{-5}$ S cm^{-1} at 130 °C under anhydrous conditions.[28]

To our idea, an enhancement of proton conductivity through a resonance structure of heterocycles i.e., benzimidazole can be achieved if the heterocycles perform favorable hydrogen bond networks and the packing structures of the polymer chains allow efficient and effective proton transfer. Based on this viewpoint, in this work, polyethylenimine containing benzimidazoles branching is originally designed since its structure offers a flexible chain with multifunctional and multidirectional proton conductive species of benzimidazoles which their hydrogen bonds can be consequently developed. It should be noted that the hydrogen bond along the structure, although enhances the conductivity, obstructs the polymer chain mobility. Therefore, an optimal level to balance the hydrogen bond network as a framework of proton transferring channel and the chain mobility as a flexible structure for proton transfer has to be identified. The present work shows the way to investigate the proton conductive performance under benzimidazole contents and temperatures profiles and clarifies how the two factors, i.e., hydrogen bonding and chain mobility, play the role in proton transfer in anhydrous system.

4.3 Experimental

4.3.1 Materials

*b*PEI (MW 25000 g mol^{-1}), hydrolyzed-poly(vinyl alcohol) (PVA, MW 89000-98000 g mol^{-1}), 2-(chloromethyl)benzimidazole (MBz), and deuterated dimethyl sulfoxide (DMSO-d_6) were obtained from Aldrich Co. *b*PEI was dried under vacuum at 80 °C for 2 days before use. Other chemicals, potassium hydroxide (KOH, Acros Co.), dimethyl sulfoxide (DMSO, Acros Co.), and hydrochloric acid (HCl, Labscan Co.) were used as received.

4.3.2 Synthesis of MPEIs (Scheme 4.1)

DMSO solution (10 ml) containing 2 g of *b*PEI (46.5 mmol) was added with an equimolar ratio of KOH to MBz. The solution was stirred and heat at 90 °C for 30 min before dropwising the DMSO solution (20 ml) containing MBz (6.4 mmol, 0.2 equivalent of primary and secondary amine contents in *b*PEI). After stirring at 90 °C under N_2 atmosphere for 24 hours, the reaction mixture was cooled down to room temperature and neutralized with 1 M HCl. The product was dialyzed in de-ionized water several times followed by freeze-drying to obtain *b*PEI containing multi-methylbenzimidazole groups, MPEI 1:0.2. In similar, MPEI 1:0.4, MPEI 1:0.6, MPEI 1:0.8, and MPEI 1:1.0 were prepared but using MBz for 0.4, 0.6, 0.8, and 1.0 mole equivalent to amine groups (primary and secondary amines) in *b*PEI, respectively.

Multi-benzimidazole functionalized branched polyethylenimine, MPEI. FTIR (KBr, ν cm^{-1}) 3600-2400 (br), 2953 (vs), 2833 (vs), 1621 (m), 1591 (w), 1534 (m), 1435 (s), 1272 (s), 746 (s). ^{1}H NMR (δ ppm, 500 MHz, DMSO-d_6, 298 K): 7.5 (s, Ar*H*), 7.1 (s, Ar*H*), 3.9 (br, N-CH_2), 2.3-2.9 (br, N-CH_2). ^{13}C NMR (δ ppm, 500 MHz, DMSO-d_6, 298 K): 152.70, 138.48, 121.45, 114.71, 51.57, 46.35, 36.93.

Scheme 4.1 Synthesis of MPEI

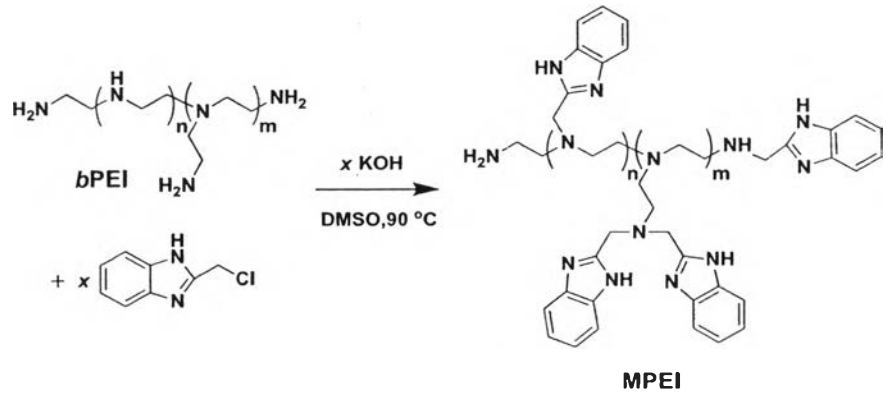

4.3.3 Preparation of MPEI/PVA membranes

The MPEI 1:0.2 in DMSO solution (10 % w/w, 1.2 ml) was mixed with DMSO containing PVA (10 % w/w, 1.8 ml) and stirred at room temperature for a day to obtain a homogeneous solution prior to cast on the glass plate with a

dimension of 3x3 cm^2. The membranes obtained were annealed at 80 °C for three days and further dried in vacuum oven at 100 °C for 1 day. Similarly, the PVA membranes containing MPEI 1:0.4, MPEI 1:0.6, MPEI 1:0.8, and MPEI 1:1.0 were prepared.

4.3.4 Characterizations

FTIR spectra of MPEIs were recorded on a Digilab FTS 7000 rapid-scan-type FTIR spectrometer with a resolution of 2 cm^{-1} for 32 scans in a frequency range of 4000-400 cm^{-1}. The temperature dependence FTIR spectra were performed using a temperature-controller attachment operating under nitrogen atmosphere. The MPEI/PVA membranes were analyzed by a Nicolet 6700 continuum in a frequency range of 4000-750 cm^{-1} with 64 scans at a resolution of 2 cm^{-1}.

^1H and ^{13}C nuclear magnetic resonance (NMR) spectra were obtained from a Bruker Avance 500 MHz NMR spectrometer. The samples were measured at 25 °C using DMSO-d_6 as a solvent.

Elementary analysis (EA) was done by a Yanako CHN CORDER to determine number of nitrogen and carbon contents for verifying degree of methylbenzimidazole substitution.

Temperature dependence wide angle X-ray diffraction (WAXD) was conducted by a Rigaku X-ray powder diffractometer/RINTTTR III Thermo plus DSC (differential scanning calorimeter) with Cu-Kα radiation (λ = 0.1542 Å). The WAXD profiles were recorded at temperature range 0-200 °C with a heating/cooling rate 3 °C min^{-1} under nitrogen atmosphere.

Thermal behaviors were observed by using a NETZSCH DSC 200 F3 Maia® at heating rate 10 °C min^{-1} under N_2 atmosphere. Thermal gravimetric analysis was carried out by using a Q5000IRS with a heating rate of 10 °C min^{-1} over temperature range of 50-650 °C under N_2 atmosphere.

The proton transfer efficiency of MPEIs with varied benzimidazole branching was comparatively studied both in pellet form of the pure MPEIs and in membrane form of the MPEI blended with PVA (MPEI/PVA membranes). In the case of MPEI pellet, the samples were dried in a vacuum oven at 80 °C for 2 days prior to press into pellet with hydraulic compression at 1.9×10^3 MPa. For MPEI/PVA

membranes, the prepared membranes were dried in a vacuum oven at 100 °C for a day before three pieces of membranes were gathered to perform proton conductivity measurement. The samples were assembled in between copper electrodes of sealed-off cylindrical Teflon cell. The resistance of the samples was determined by complex impedance method with a μAUTOLAB Type III potentiostat/galvanostat in a frequency range from 500,000 to 0.01 Hz and ac signal amplitude of 50 mV. The measurements were carried out in the temperature range of 50-190 °C under temperature and humidity controls. The conductivity (σ) is calculated from impedance data by using eq 1;

$$\sigma = (1/R) \cdot (L/A) \quad (1)$$

where L is the sample thickness, A is the cross-sectional area between membrane and electrode and R is the resistance derived from the intersection of Nyquist plot on real axis at imaginary part equal to zero.

4.4 Results and Discussion

4.4.1 Synthesis and structural characterization of MPEIs

A series of benzimidazole branching with different benzimidazole contents were prepared by varying the molar ratios of MBz to *b*PEI through nucleophilic substitution of alkyl chloride with basic amines of *b*PEI in the presence of KOH in DMSO solution under N_2 atmosphere. The yields of the products are as high as 76-90 % (Table 4.1).

Table 4.1 Effect of *b*PEI:MBz feeding ratios to % yield of the products, percent contents of hydrogen, carbon and nitrogen and calculated degree of substitution

Samples	Feeding ratio of *b*PEI:MBz	Yield (%)	Elemental Compositions (%)			DS (%)
			H	C	N	
MPEI 1:0.2	1:0.2	90	8.36	48.79	23.32	19.7
MPEI 1:0.4	1:0.4	81	7.10	51.03	21.73	41.4
MPEI 1:0.6	1:0.6	88	6.56	52.96	21.69	51.5
MPEI 1:0.8	1:0.8	85	6.62	56.52	22.19	66.7
MPEI 1:1.0	1:1.0	76	6.61	62.47	23.34	90.5

FTIR spectra of the MPEIs show the characteristic absorption bands of benzimidazole structure at 1621 cm^{-1} (C=N deformation mode), 1534 cm^{-1} (N-H deformation mode), 1435 cm^{-1} (in-plane vibration), and 746 cm^{-1} (C-H bending mode). The broad absorption bands at 3600-2400 cm^{-1} are assigned to the hydrogen bonded N-H. The peaks at 2953 and 2833 cm^{-1} clearly indicate C-H stretching mode of *b*PEI chain.

Figure 4.1a shows an example of ^1H NMR spectrum of MPEI 1:0.6. The chemical shift of CH_2-Cl at 4.93 ppm belonging to chloromethylbenzimidazole does not appear and this indicates a successful functionalization of *b*PEI with methylbenzimidazole groups. The signals at 2.3-2.9 ppm corresponding to H_1, H_2, and H_3 along *b*PEI chain and the signals at 7.1 and 7.5 ppm corresponding to H_6 and H_7 in the benzimidazole ring are observed. A broad chemical shift with the center at 3.9 ppm is assigned to the protons (H_4 and H_5) between nitrogen atom and benzimidazole ring.

The broad chemical shift of ^1H NMR spectrum in the range of 2.0-4.0 ppm as a result of the overlapping between the sample and solvent peaks limits a definitive assignment of the polymer obtained, therefore, ^{13}C NMR spectrum was further investigated (Figure 4.1b). The spectrum shows the downfield signals at 51.57, 46.35 and 36.93 ppm corresponding to the methylene carbons adjacent to

tertiary (C_1 and C_4), secondary (C_2 and C_5), and primary (C_3) amines, respectively. The upfield signals at 121.45 and 114.71 ppm are corresponding to methine carbons (C_6 and C_7), and the ones at 138.48 and 152.70 ppm are quaternary carbons (C_8 and C_9) of benzimidazole ring.

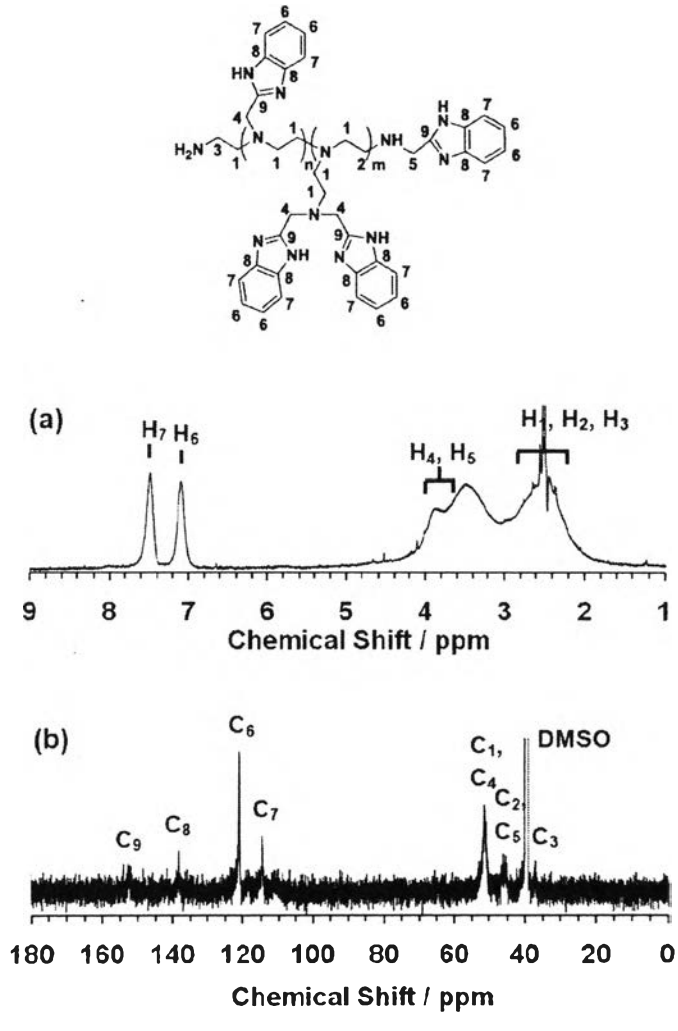

Figure 4.1 (a) ^{1}H NMR and (b) ^{13}C NMR spectra of MPEI 1:0.6 (labeled numbers on MPEI structure identifying the positions of hydrogen and carbon in the NMR spectra).

To identify proton and carbon connectivity, 2D correlation NMR spectra (edited-HSQC (Heteronuclear Single Quantum Correlation)) of ^{1}H and ^{13}C DEPT-

135 (Distortionless Enhancement by Polarization Transfer) were applied. For example, HSQC spectrum of MPEI 1:0.6 (Figure 4.2) proves that methylbenzimidazoles are attached to amine groups to form tertiary and secondary amines as evidenced from the cross peaks at F and G, respectively. The correlations between protons and methylene carbons of *b*PEI connected to tertiary, secondary and primary amines are found at C, D and E, respectively. In addition, the cross peaks belonging to the correlation of methine carbons of benzene ring and aromatic protons are found at A and B.

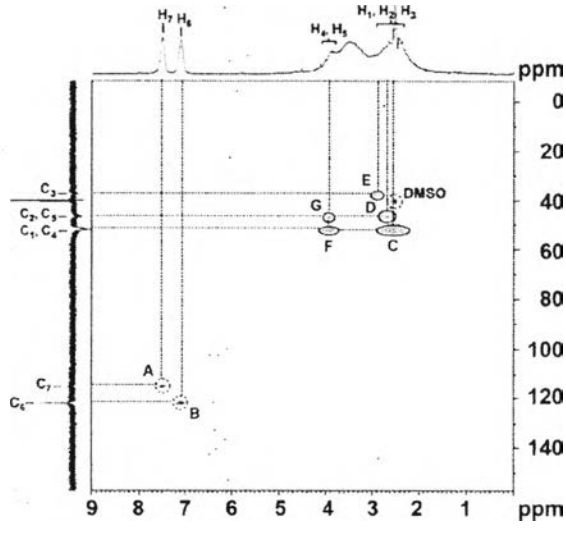

Figure 4.2 ^{1}H-^{13}C DEPT-135 edited-HSQC spectrum (solid line = negative phase peak and dash line = positive phase peak).

*b*PEI (M_n = 10000 g.mol^{-1}) was obtained from Aldrich Co. *b*PEI consists of terminal end group primary amine (T), linear secondary amine (L) and dendritic tertiary amine (D). Amine compositions were calculated from a quantitative analysis of ^{13}C NMR using an inverse gated ^{1}H decoupling with a delay time of 10 s. ^{13}C NMR spectrum of *b*PEI (Figure 4.3) was recorded using D_2O as a solvent. The percent contents of T, L, and D units were estimated according to Appelhans et al.[30] as follows.

$$T = (I_a + I_b)/I_{total} \cdot 100 \quad (2)$$

$$L = 1/2 \cdot (I_c + I_d + I_e)/I_{total} \cdot 100 \quad (3)$$

$$D = 1/3 \cdot (I_f + I_g + I_h)/I_{total} \cdot 100 \quad (4)$$

where T, D, and L are the contents of tertiary, secondary and primary amines in percent, respectively. I_i is ^{13}C NMR signal intensity at position i, $I_f = I$ (48-50 ppm) - I_b, and $I_{total} = (I_a + I_b) + 1/2 \cdot (I_c + I_d + I_e) + 1/3 \cdot (I_f + I_g + I_h)$.

Figure 4.3 shows the peaks belonging to I_a, and I_b with a relative intensity for 1.99 as compared to I_h. By substituting I_a and I_b in eq 2, T value was found to be 31.0 % (T=1.99/6.42·100). Similarly, I_c, I_d, and I_e show a relative intensity for 5.19 whereas I_f, I_g, and I_h show a relative intensity for 5.49 as compared to I_h to represent L, and D, respectively. By substituting I_c, I_d, and I_e in eq3 and I_f, I_g, and I_h in eq 4, L and D values were found to be 40.5 % (L=(1/2·5.19)/6.42*100) and 28.5 % (D=(1/3·5.49)/6.42*100), respectively.

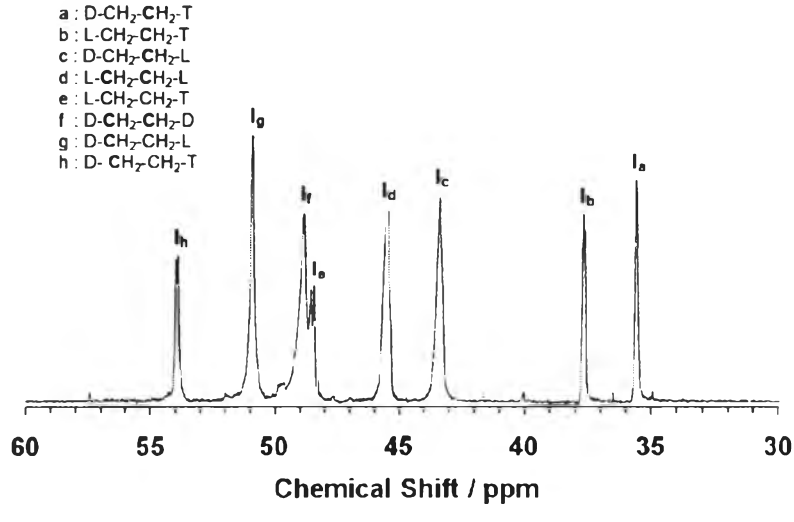

Figure 4.3 Inverse gated ^{13}C NMR spectrum of *b*PEI.

Therefore, T = 31.0 %, L = 40.5 %, and D = 28.5 %.

Degree of polymerization (DP): DP = $M_n/M(CH_2CH_2NH)$ = 10000/43 = 232
The approximate numbers of T, L, and D per polymer chain were found to be 72, 94 and 66, respectively.

The degree of methylbenzimidazole substitution (DS) on the *b*PEI chain was calculated by means of eq 5 and eq 6.[29]

$$N/C = ((14 \cdot 232) + (x \cdot 2 \cdot 14))/((2 \cdot 12 \cdot 232) + (x \cdot 8 \cdot 12)) \quad (5)$$

$$DS\ (\%) = x/(T+L) \cdot 100\ \% \quad (6)$$

where N and C are the number of nitrogen and carbon contents obtained from elemental analysis, x is the number of methylbenzimidazoles functionalized on *b*PEI chain, T is the number of terminal primary amines ($-NH_2$), and L is the number of linear secondary amines (-NH-) based on quantitative ^{13}C NMR analysis.

The elemental compositions and percent DS under variation of *b*PEI:MBz ratios are in Table 4.1. When the feed ratios were varied from 1:0.2 to 1:1.0, the degrees of substitution are changed from 19.7 % to 90.5 %. It should be noted that the substitution is almost equal to that of the feed ratio, in other words, the degree of benzimidazole substitution on *b*PEI can be controlled by simply varying the ratio of *b*PEI:MBz.

4.4.2 Thermal properties of MPEIs

Thermal gravimetric analysis (TGA) was used to investigate thermal stability of the MPEIs. Table 4.2 summarizes the degradation temperature (T_d) and percent residue of MPEIs as compared with *b*PEI. All types of MPEIs show the first weight loss starting from ~67 °C (onset temperature) to ~100 °C attributed to the loss of the absorbed moisture. The onset T_d around 280-290 °C at the weight loss for less than 8 % suggests the degradation of methylbenzimidazole pending group and polyethylenimine backbone. Although the MPEIs shows the lower thermal stability than that of the *b*PEI (T_d = 327 °C), their degradation temperatures are still much

higher than the operating temperature of PEMFC, i.e., at around 150 °C. The residue (3.0-5.8 wt %) might come from some chloride-based salts remained. An additional confirmation by analyzing TGA of MBz confirmed the ash content as high as 30 wt %. No ash content is observed in the case of the pure benzimidazole compound.

Table 4.2 T_d, percent residue, and T_g of the MPEIs compared with *b*PEI

Samples	T_d (°C)	Residue (%)	T_g (°C)
*b*PEI	327.2	0	-49.3
MPEI 1:0.2	280.2	3.0	42.8
MPEI 1:0.4	290.4	2.6	80.7
MPEI 1:0.6	291.4	5.8	100.8
MPEI 1:0.8	285.7	3.7	107.0
MPEI 1:1.0	286.6	4.8	107.7

In the temperature range from -90 °C to 200 °C, the DSC thermograms of MPEIs during the 2nd heating at 10 °C min^{-1} show only a glass transition temperature (T_g) without melting temperature. Here, the T_gs were used to clarify an ease of chain movement. It is important to emphasize that MPEIs show a dramatically increase of T_g as compared with *b*PEI (from -49.3 °C to more than 42.8 °C, Table 4.2) implying a decrease of polymer chain flexibility or free volume of the modified polymers. The T_gs of MPEIs are ranging from 42.8 °C to 107.7 °C depending on percent DS. MPEI 1:0.2 with the lowest contents of benzimidazoles (19.7 % DS) shows the lowest T_g at 42.8 °C. In other words, the lower percent DS is, the more chain mobility will be. However, after the percent DS was above 51.5 %, the increase of T_g is not significant. The similar results were also observed in the case of benzimidazole-tethereded polysiloxanes as reported by Perssson et al.[16]

4.4.3 Hydrogen bond interaction of MPEIs traced by temperature dependence FTIR

In order to verify how benzimidazole substitution degree induces the changes of hydrogen bond performance under various temperatures, FTIR measurements in the temperature range of 30-200 °C with 3 steps of heating-cooling-

heating conditions under N_2 atmosphere were done. Because the hydrogen bond directly relates to proton transfer,[12] the broad absorption bands from 3600 to 2400 cm^{-1} assigned to N-H stretching mode under inter- and intramolecular H-bonding were focused to determine the effect of temperature to hydrogen bond interaction. Figure 4.4 shows FTIR spectra of MPEI 1:0.2 at variable temperatures during the 1st heating (Figure 4.4a), followed by cooling (Figure 4.4b), and ending with 2nd heating (Figure 4.4c)) processes. The broad absorption intensity at 3600-2400 cm^{-1} significantly decreases during the 1st heating step which corresponds to the reduction of hydrogen-bound water as identified by TGA. The broad hydrogen-bonded N-H intensity gradually increases during cooling indicating the recovering of hydrogen bond interaction. The intensity decreases again during the 2nd heating process implying reversible hydrogen bond formation during heating and cooling.

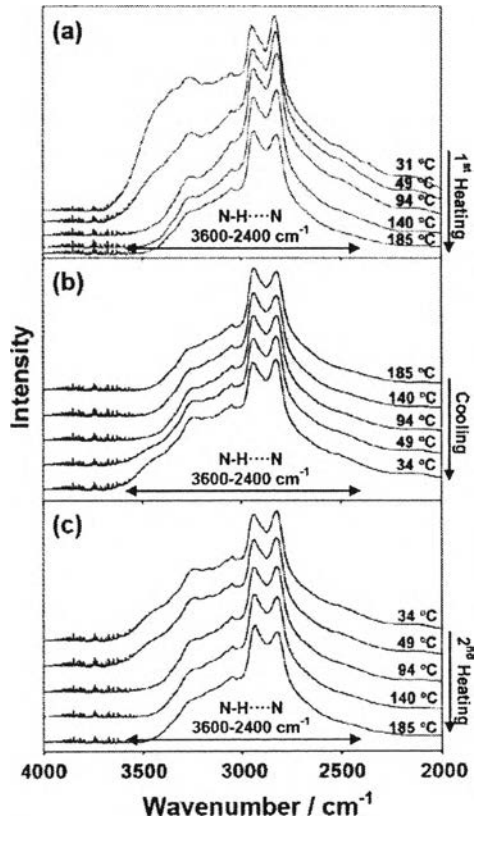

Figure 4.4 Temperature dependence FTIR spectra of MPEI 1:0.2 during (a) 1st heating, (b) cooling, and (c) 2nd heating.

To determine the changes of hydrogen bond related to temperature in the polymer structures without interruption of water, the FTIR spectra during the second heating process were carefully investigated. The broad peaks from 3600 cm^{-1} to 2400 cm^{-1} continuously decrease during an increase of temperature (Figure 4.5).

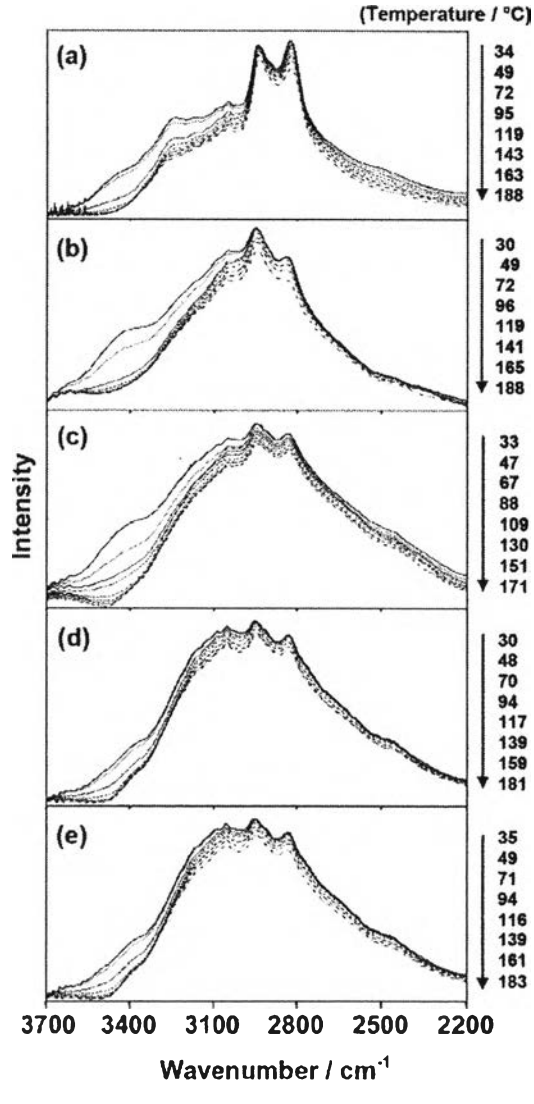

Figure 4.5 Temperature dependence FTIR spectra of (a) MPEI 1:0.2, (b) MPEI 1:0.4, (c) MPEI 1:0.6, (d) MPEI 1:0.8, and (e) MPEI 1:1.0 during the second heating process.

In order to trace the hydrogen bond changes, a quantitative analysis of hydrogen bond by FTIR was clarified. It should be noted that the broad absorption region (3600-2400 cm^{-1}) covers the strong absorption intensities of CH_2 stretching modes at 2953 cm^{-1} and 2833 cm^{-1}, therefore; in order to quantitatively compare the number of hydrogen bond of MPEIs, the broad peak area from 3600 cm^{-1} to 2400 cm^{-1} was subtracted with the peak areas of CH_2 stretching. The peak areas were quantified by curve fitting technique using OPUS 5.5 program (Figure 4.6).

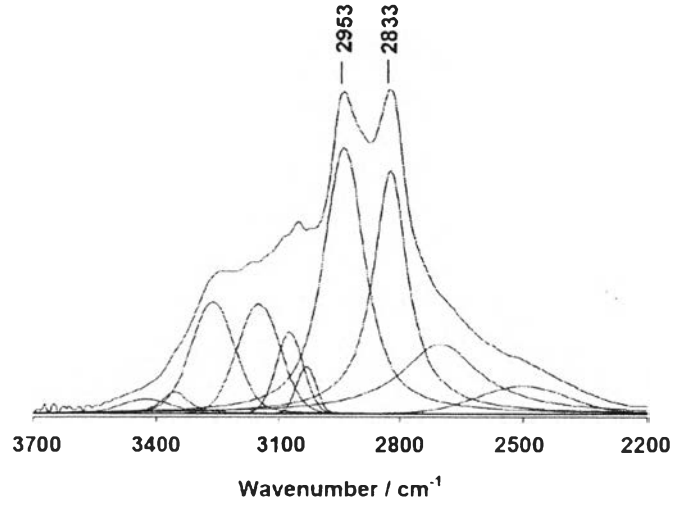

Figure 4.6 FTIR curve fitting of MPEI 1:0.2.

The values of the subtracted peak areas divided by the peak areas of CH_2 stretching i.e., $[A_{3600\text{-}2400}\text{-}(A_{2953}+A_{2833})]/(A_{2953}+A_{2833})$ give us the information about the relative amount of H-bond. As shown in Figure 4.7, MPEI 1:0.2 with the lowest benzimidazole substitution exhibits the lowest hydrogen bond concentration and the lowering of H-bond during an increase of temperature. A similar behavior was also observed for other MPEIs under temperature variation.

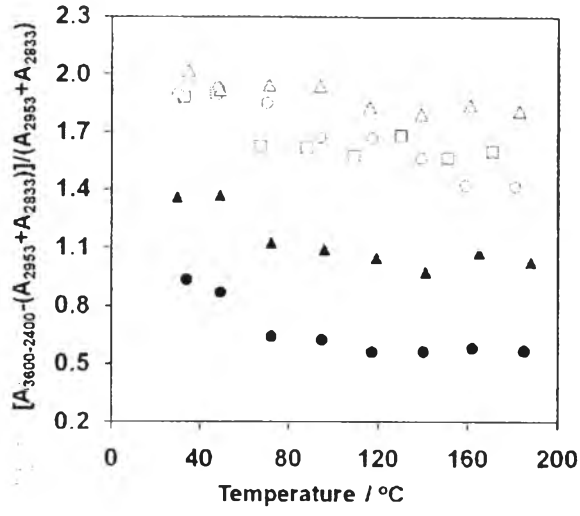

Figure 4.7 Semi-quantitative analysis of hydrogen bond network based on FTIR spectra of MPEI 1:0.2 (●), MPEI 1:0.4 (▲), MPEI 1:0.6 (□), MPEI 1:0.8 (○), and MPEI 1:1.0 (△) (Calculated from those of Figure 4.5).

The MPEIs with higher percent DS show the more significant H-bond, and when the substitution of benzimidazole groups reached a certain amount as seen in the cases of MPEI 1:0.6, MPEI 1:0.8, and MPEI 1:1.0, the quantitative evaluation of hydrogen bond shows the similar values in the range of 1.4-2.0. Combining with the glass transition temperature analyzed by DSC (Table 4.2), it is clear that the more heterocycles conjugated onto *b*PEI not only initiate the more hydrogen bond network but also perform the less chain mobility.

4.4.4 Study on morphology under temperature variation based on temperature dependence WAXD

Temperature dependence WAXD was performed to study the morphology changes related to temperature. During the second heating at 3 °C.min^{-1}, MPEIs show the broad WAXD patterns shifted to the lower angle (Figure 4.8). Radial distribution function (RDF) which can be calculated from the WAXD patterns is a good evaluation to see how the polymer chains perform the packing under various temperatures. The temperature dependence RDF reflects the probability to find the

atomic distribution in spherical shell of radius r around one centered atom with respect to temperature.

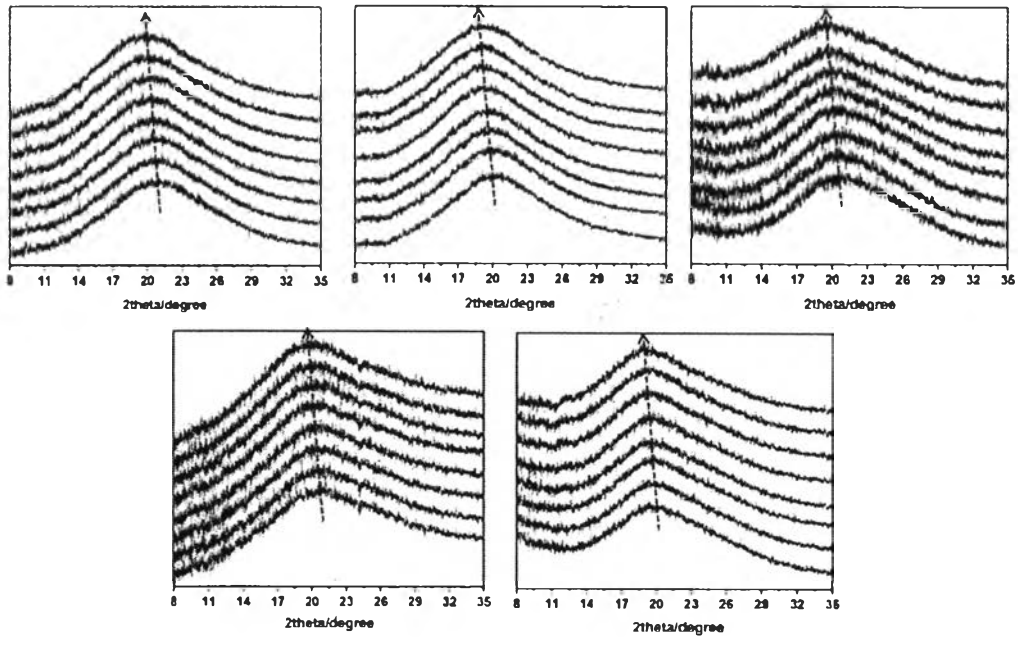

Figure 4.8 WAXD profiles under temperature variation of (a) MPEI 1:0.2, (b) MPEI 1:0.4, (c) MPEI 1:0.6, (d) MPEI 1:0.8, and (e) MPEI 1:1.0.

The powder diffraction intensities, I(q), were corrected with background including incoherent scattering, polarization (P), and Lorentz (L) factors according to the follows.[31-34]

$$P = (1 + \cos^2 2\theta_M \cos^2 2\theta)/2 \quad (7)$$

$$L = 1/\sin 2\theta \sin\theta \quad (8)$$

$$I(q) = k \cdot I_{coh}(q) - x_i f_i^2(q) \quad (9)$$

$$i(q) = I(q)/\sum x_i f_i^2(q) \quad (10)$$

$$i(q) = k[I_{coh}(q)/\sum x_i f_i^2(q)] - 1 \quad (11)$$

where θ_M is the Bragg's angle of the reflection from the monochromator, θ is the angle between the X-ray beam and the planes, I_{coh} is the coherent scattering intensity, x_i is the mole fraction obtained from elementary analysis and $f_i(q)$ is the atomic scattering factor of species i calculated from $f(\sin\theta/\lambda) = \sum a_i \cdot \exp[-b_i \cdot (\sin\theta/\lambda)^2] + C$, and $k = 0.4142/(FWHM/2)^2$. Fourier transformation of i(q) leads to a formation of radial distribution function, g(r), as follow:

$$g(r) = 4\pi r^2[\rho(r) - \rho_o] = (2r/\pi) \cdot \int q \cdot i(q) \cdot M(q) \cdot \sin(qr)dq \quad (12)$$

Here, ρ_o is the average density of atoms in the sample, $\rho(r)$ is the number of atoms per unit volume at a distance r from the reference atom, q is scattering vector, $q = 4\pi\sin\theta/\lambda$, and M(q) is the window function, $M(q) = \sin(\pi q/q_{max})/(\pi q/q_{max})$.

Figure 4.9 shows the RDFs as a function of temperature for MPEIs. As the WAXD profiles were recorded in the region of 8° to 35° 2θ, the distance at r between 2.6 Å and 11.0 Å in the temperature range of 0 °C - 200 °C was focused. It is important to note that the significant changes of the atomic distribution related to temperature can be observed at the r distance from 4.4 Å to 6.1 Å. An increase of temperature results in a decrease of the peak at r = 4.4 Å and an increase of the peak at r = 6.1 Å. This tendency was found in most of MPEIs. The peak at 4.4 Å might refer to the N-H···N hydrogen bonded atomic pairs judging from the temperature dependence of N-H···N stretching peak in FTIR spectra (Figure 4.5). For an increase of the peak at 6.1 Å, as the distance is much larger than the hydrogen bonding, the peak might come from many possibilities, for example the local packing structure, especially the benzimidazole packing.

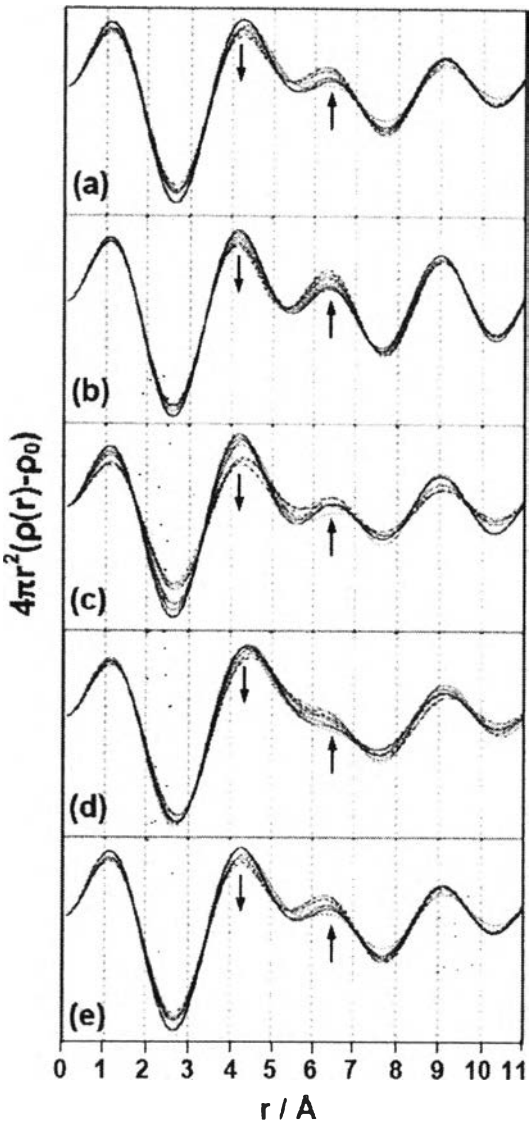

Figure 4.9 Radial distribution functions of (a) MPEI 1:0.2, (b) MPEI 1:0.4, (c) MPEI 1:0.6, (d) MPEI 1:0.8, and (e) MPEI 1:1.0 at approximate temperature 30 °C (——), 50 °C (·····), 75 °C (--------), 100 °C (- - - -), 125 °C (-·-·-·-), 150 °C (– – –), 175 °C (– · – ·), and 200 °C (– · · –).

4.4.5 Proton conductivity of MPEIs

To directly investigate the proton transfer efficiency of the MPEIs obtained, the samples were compressed as pellets and the proton conductivities were verified by using impedance spectroscopy technique. It is important to note that among all

MPEIs only two types, i.e., MPEI 1:0.2 and MPEI 1:0.4, show the proton conductivity (Figure 4.10). This might imply an effective amount of benzimidazole subsitution (19.7-41.4 %) in the system which the hydrogen bond and chain flexibility are in good balance to favor the proton transfer. For both samples, an increase of temperature results in an increase of proton conductivity. The maximal values are $1.3x10^{-5}$ S cm^{-1} and $1.7x10^{-5}$ S cm^{-1} at 190 °C for MPEI 1:0.2 and MPEI 1:0.4, respectively. Combining with the temperature dependence WAXD and FTIR, it is reasonable to mention that, during an increase of temperature, the rearrangement of the atoms with a higher inter-atomic distance distribution causes the reduction of hydrogen bond and consequently results in an increase of proton conductivity. The conductivities of the MPEI 1:0.2 and MPEI 1:0.4 were compared with that of Nafion®. Although the Nafion® shows the higher proton conductivity than the MPEIs, its conductivity gradually decreases above 110 °C which might be related to the loss of water molecules existed in the membrane. It should also be noted that both MPEIs maintain their proton conductivities at high temperature. This confirms the role of benzimidazoles in MPEIs for proton transferring.

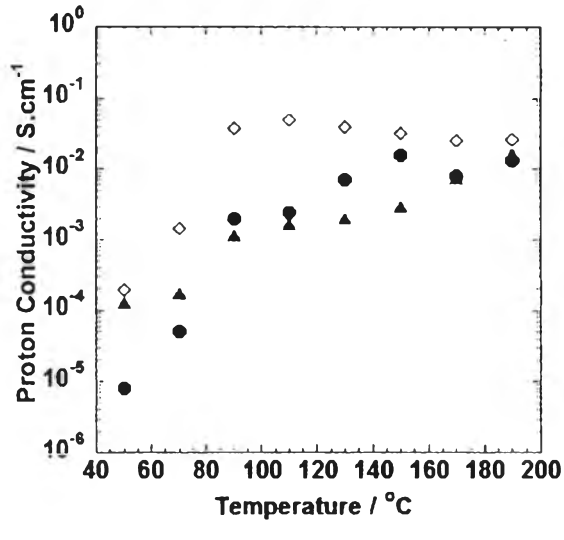

Figure 4.10 Proton conductivity of Nafion® (◇), MPEI 1:0.2 (●), and MPEI 1:0.4 (▲) as a function of temperature.

4.4.6 MPEI/PVA membranes: Study on transition temperature and hydrogen bond network

Since the pristine MPEIs were difficult to form membranes, an attempt to blend MPEIs with other polymers was carried out. It was found that PVA was appropriate because it shows a miscible blend with MPEIs. DSC thermogram of each blend membrane shows a single T_g indicating the miscibility between MPEIs and PVA (Figure 4.11). The glass transition temperatures continously increase from 42.3 °C to 83.4 °C for MPEI 1:0.2 to MPEI 1:1.0. In other words, the T_g increases with an increase of benzimidazole branches. The increment of T_g implies the more significant interaction of MPEI with PVA when MPEI has more branching units.

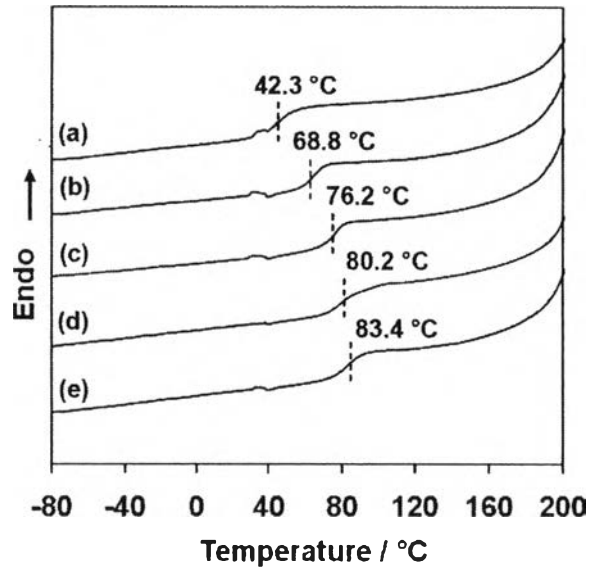

Figure 4.11 DSC thermograms of (a) MPEI 1:0.2/PVA, (b) MPEI 1:0.4/PVA, (c) MPEI 1:0.6/PVA, (d) MPEI 1:0.8/PVA, and (e) MPEI 1:1.0/PVA during the second heat treatment at heating rate 10 °C min^{-1} under N_2 atmosphere.

The FTIR spectra of the blend membranes clarify the hydrogen bond interaction between MPEI and PVA. The PVA characteristic peaks at 1091 cm^{-1} (out-of-phase C-C-O stretching mode) and 2941 cm^{-1} and 2911 cm^{-1} (C-H stretching mode) are maintained at the same position even after blending with MPEIs (Figure 4.12). The OH stretching bands (3000-3600 cm^{-1}) of PVA in the blends clearly shift

to the higher wavenumber indicating the weakening of O-H···O bonds. This implies the change of hydrogen bonded patterns of PVA from O-H···O to be the partial O-H···N and N-H···N of MPEI. Figure 4.13 illustrates the case that the H-bond formation of PVA and of MPEI develops the hydrogen bond network.

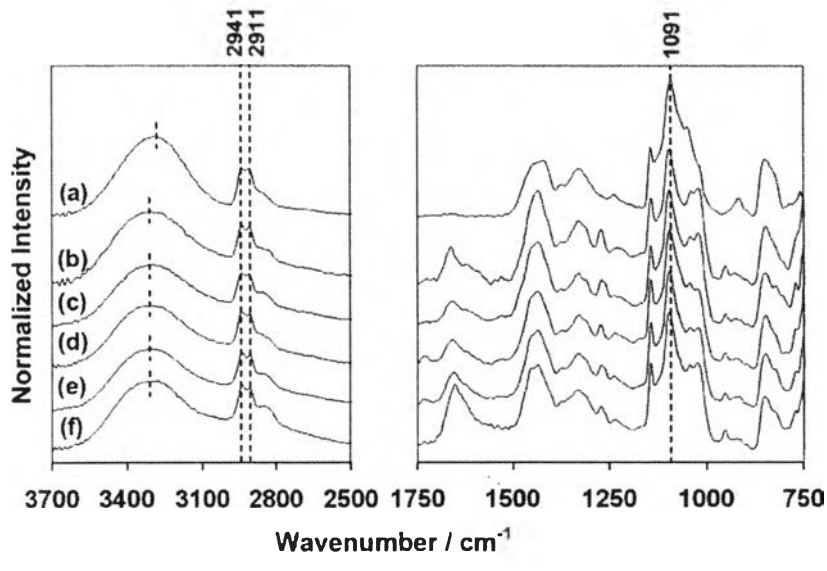

Figure 4.12 FTIR spectra of (a) PVA, (b) MPEI 1:0.2/PVA, (c) MPEI 1:0.4/PVA, (d) MPEI 1:0.6/PVA, (e) MPEI 1:0.8/PVA, and (f) MPEI 1:1.0/PVA membranes measured at room temperature.

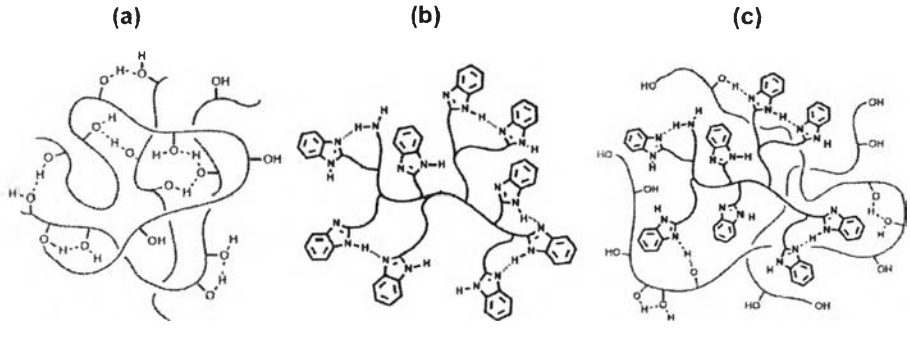

Figure 4.13 Possible hydrogen bond formation of (a) PVA, (b) MPEI, and (c) MPEI/PVA membranes.

4.4.7 Proton transfer efficiency of MPEI/PVA membranes

As the present work focuses on anhydrous PEM system, the proton conductivities were measured at the second heating process to ensure the complete moisture exclusion. Figure 4.14 shows the proton conductivities of MPEI/PVA membranes as compared to that of PVA in the temperature range 90-190 °C. The proton conductivity of PVA becomes greater after adding MPEIs. As mentioned above, the conductivity of each MPEI was evaluated directly by pressing the samples as pellets and at that time the conductivities of MPEI 1:0.6, MPEI 1:0.8, and MPEI 1:1.0 were not identified. However, after mixing with PVA, MPEI 1:0.6, MPEI 1:0.8, and MPEI 1:1.0 showed conductivity significantly. This indicates that the polymer matrices play the role to support MPEIs for the proton conduction. In addition, all samples perform an increase of proton conductivity with temperature. The MPEI 1:0.2/PVA and MPEI 1:0.4/PVA membranes with the low percent DS exhibit the proton conductivity at the level of 10^{-4} S cm^{-1} at 190 °C whereas others show the maximum conductivity at the level of 10^{-5} S cm^{-1}.

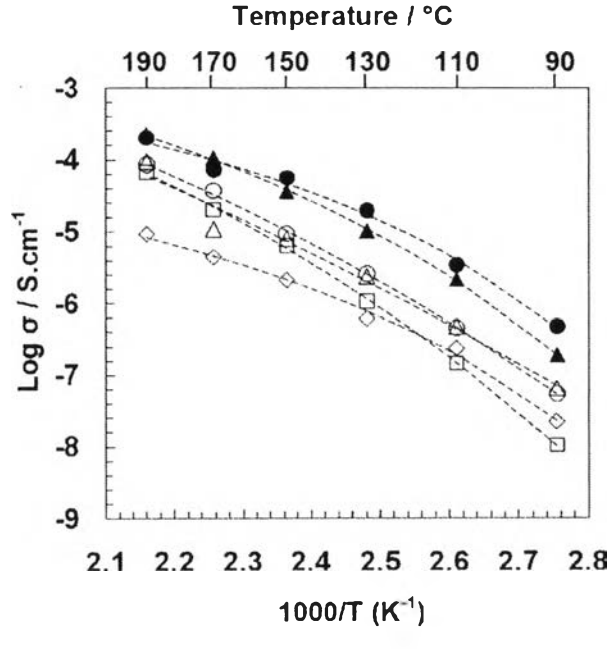

Figure 4.14 Arrhenius plot of proton conductivity comparing the experimental data of PVA (◇), and PVA blended with MPEI 1:0.2 (●), MPEI 1:0.4 (▲), MPEI 1:0.6

(□), MPEI 1:0.8 (○), and MPEI 1:1.0 (△) membranes with the value obtained from VTF equation fitting (dash lines) during the second heating process.

The temperature dependence proton conductivities of MPEI/PVA membranes show a curve deviation from linear relationship between proton conductivity and reciprocal temperature. Consequently, the conductivities at various temperatures were fitted to Vogel–Tamman–Fulcher (VTF) equation to estimate activation energy for proton transfer as follow.

$$\log \sigma = \log \sigma_o - (E_a/R(T-T_0)) \quad (10)$$

where σ is the proton conductivity at a particular temperature (S cm^{-1}), σ_o is the pre-exponential factor that represents the conductivity at infinite temperature (J mol^{-1}), E_a is activation energy for proton transfer (J mol^{-1}), R is gas constant (8.314 J K^{-1} mol^{-1}), T is the absolute temperature (K), and T_0 is the Vogel temperature which is the point that there is no change of configurational entropy in the polymer.[35] Here, the VTF parameters obtained from the curve fitting i.e., E_a, σ_0, and T_0 are summarized in Table 4.3.

Table 4.3 Parameters obtained from curve fitting of temperature dependence proton conductivity with VTF equation

Samples	VTF parameters			
	E_a (kJ/mol)	σ_0 (S/cm)	T_0 (°K)	R^2
PVA	3.12	0.001	282	0.9950
MPEI 1:0.2/PVA	2.78	0.015	289	0.9924
MPEI 1:0.4/PVA	4.83	0.200	266	0.9960
MPEI 1:0.6/PVA	9.66	6.816	231	0.9996
MPEI 1:0.8/PVA	10.47	7.909	189	0.9994
MPEI 1:1.0/PVA	15.38	65.62	157	0.9759

The Arrhenius plots were well fitted with VTF behavior (dash line in Figure 4.14) with the correlation coefficient, R^2 value, for 0.9759-0.9996. This indicated that the proton transfer behavior is mainly controlled by segmental motion of the polymer.[36] The E_a values of MPEI/PVA membranes are around 2.78-15.38 kJ mol^{-1} which are in the same range with other benzimidazole based structures. For example, Persson et al. reported that benzimidazole oligomers containing two and ten ethylene oxide units showed E_a values 8.2 kJ mol^{-1} and 4.2 kJ mol^{-1}, respectively[10] and He et al. reported that polybenzimidazole doped with H_3PO_4 showed the activation energy for 8-11 kJ mol^{-1}.[37] In our case, MPEI 1:0.2/PVA shows the lowest activation energy for proton transfer, and the activation energy increases in the order of MPEI 1:0.2 < MPEI 1:0.4 < MPEI 1:0.6 < MPEI 1:0.8 < MPEI 1:1.0. This suggests how benzimidazole branching improves proton transfer performance in the polymer blend membrane.

4.4.8 Proton transfer performance under a balance of hydrogen bond and chain mobility

Figure 4.15 illustrates the overlaid re-plots of proton conductivty in addition to glass transition temperature and relative amount of hygrogen bond as a function of percent DS to determine how proton transfer related to the hydrogen bond and the mobility of the polymers. It is clear that MPEIs with the more percent DS tend to show a decrease of proton conductivity as a result of the more hydrogen bond network. The hydrogen bond network might retard the free chain movement and reduce proton transfer efficiency. Up to a particular point, the lowest proton conductivity was observed in the case of MPEI 1:0.6 with DS 51.5 %. However, it is also clear that MPEI 1:0.8 and MPEI 1:1.0 with the DS > 66.7 % perform a small increment of proton conductivity as compared to MPEI 1:0.6. This confirms that the hydrogen bond network more or less plays an important role in proton conductivity. But the fact that the dense hydrogen bond initiates the fixation of polymer matrices to be in a network with less chain mobility, the proton conductivity under proton movement on the chain is, therefore, in unfavorable condition. Therefore, a good balance of hydrogen bond and chain mobility is a key factor to induce an effective

proton transfer. In our case, a good balance is identified for MPEI 1:0.2 and MPEI 1:0.4 with DS 19.7-41.4 %.

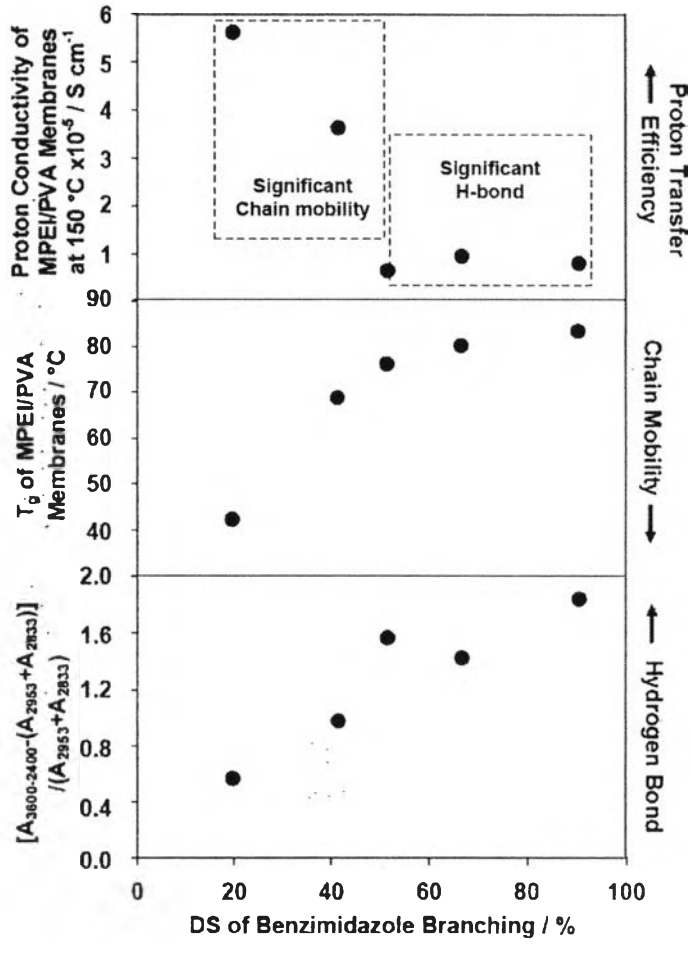

Figure 4.15 Overlaid re-plots of proton conductivity, glass transition temperature, and relative amount of H-bond as a function of DS.

4.5 Conclusions

Ideally, the favorable hydrogen bond network combining with flexible polymer chain initiates an effective proton transfer. However, the fact that the more number of hydrogen bond networks are formed, the less chain mobility will be. This

brings us to a question how we can observe a balance of both factors and declare the relationship between these factors and proton transfer performance. Here, branching benzimidazole was a good model compound to enable us to study the effect of hydrogen bond as well as the chain mobility related to the proton conductivity under the varied temperatures. The present work showed a simple synthesis of branching benzimidazoles by functionalizing the benzimidazoles onto amine groups of the *b*PEI. The substitution of methylbenzimidazole is almost relevant to the feed ratio resulting in degree of substitution in the range of 19.7-90.5 %. By following the hydrogen bond interaction under the varied temperatures with temperature dependence systems of FTIR and WAXD, including thermal analyses, the performance of proton transfer can be clarified. Based on the effect of benzimidazole content to hydrogen bond network and glass transition temperature, the higher the degree of substituted benzimidazole on branched polyethylenimine is, the higher the number of hydrogen bond and the less chain mobility will be. The proton conductivities of MPEIs showed that the proton transfer efficiency can be enhanced when i) the chain mobility is sufficiently high to allow proton hopping as in the cases of MPEIs with DS 19.7-41.4 %, and ii) the number of hydrogen bond is significant as observed from a small increment of the proton conductivity of MPEIs with DS more than 66.7 % as compared with MPEI 1:0.6 with DS 51.5 %. A good balance of hydrogen bond network and chain mobility to favor the proton transfer was found in MPEI 1:0.2 and at that time the proton conductivity of the blend membrane was as high as 10^{-4} S cm^{-1} at 190 °C under anhydrous system. Although the conductivity for 10^{-4} S cm^{-1} is not that high, the model compounds lead us to an understanding of good molecular design with a balance of benzimidazole units and their hydrogen bond networks. A systematic study on polymer chains conjugated with benzimidazole units in a series of branching network is under progress.

4.6 Acknowledgements

The research was supported by the National Research Council of Thailand and the Higher Education Research Promotion and National Research University Project of Thailand, Office of the Higher Education Commission (EN276B). One of

the authors, A. Pangon, would like to acknowledge the scholarships from the Development and Promotion of Science and Technology Talents Project (DPST) and Japan Student Services Organization (JASSO).

4.7 References

1. Barbir, F.; Gomez, T. *Int. J. Hydrogen Energy* 1996, *21*, 891-901.
2. Smitha, B.; Sridhar, S. *J. Membr. Sci.* **2005**, *259*, 10–26.
3. Candusso, D.; Harel, F.; Bernardinis, A. D.; François, X.; Péra, M. C.; Hissel, D.; Schott, P.; Coquery, G.; Kauffmann, J.-M., *Int. J. Hydrogen Energy* **2006**, *31*, 1019–1030.
4. Mauritz, K. A.; Moore, R. B. *Chem. Rev.* **2004**, *104*, 4535-4585.
5. Hickner, M. A.; Ghassemi, H.; Kim, Y. S.; Einsla, B. R.; McGrath, J. E. *Chem. Rev.* **2004**, *104*, 4587-4612.
6. Rikukawa, M.; Sanui, K. *Prog. Polym. Sci.* **2000**, *25*, 1463-1502.
7. Li, Q.; He, R. H.; Jensen, J. O.; Bjerrum, N. J. *Chem. Mater.* **2003**, *15*, 4896-4915.
8. Gosalawit, R.; Chirachanchai, S.; Manuspiya, H.; Traversa, E. *Catal. Today* **2006**, *118*, 259–265.
9. Kreuer, K. D.; Fuchs, A.; Ise, M.; Spaeth, M.; Maier, J. *Electrochim. Acta* **1998**, *43*, 1281-1288.
10. Persson, J. C.; Jannasch, P. *Chem. Mater.* **2003**, *15*, 3044-3045.
11. Asensio, J. A.; Borrós, S.; Gómez-Romero, P. *Electrochem. Com.* **2003**, *5*, 967–972.
12. Münch, M.; Kreuer, K. D.; Silvestri, W.; Maier, J.; Seifert, G. *Solid State Ionics* **2001**, *145*, 437-443.
13. Bouchet, R.; Siebert, E. *Solid State Ionics* **1999**, *118*, 287–299.
14. Asensio, J. A.; Borrós, S.; Gómez-Romero, P. *J. Polym. Sci., Part A: Polym. Chem.* **2002**, *40*, 3703-3710.
15. Xiao, L.; Zhang, H.; Scanlon, E.; Ramanathan, L. S.; Choe, E.-W.; Rogers, D.; Apple, T.; Benicewicz, B. C. *Chem. Mater.* **2005**, *17*, 5328-5333.

16. Persson, J. C.; Jannasch, P. *Macromolecules* **2005**, *38*, 3283-3289.

17. Persson, J. C.; Josefsson, K.; Jannasch, P. *Polymer* **2006**, *47*, 991–998.

18. Persson, J. C.; Jannasch, P. *Chem. Mater.* **2006**, *18*, 3096-3102.

19. Woudenberg, R. C.; Yavuzcetin, O.; Tuominen, M. T.; Coughlin, E. B. *Solid State Ionics* **2007**, *178*, 1135–1141.

20. Yamada, M.; Honma, I. *Electrochim. Acta* **2003**, *48*. 2411-2415.

21. Yamada, M.; Honma, I. *Polymer* **2005**, *46*, 2986–2992.

22. Karadedeli, B.; Bozkurt, A.; Baykal, A. *Physica B* **2005**, *364*, 279–284.

23. Bozkurt, A.; Meyer, W. H.; Wegner, G. *J. Power Sources* **2003**, *123*, 126–131.

24. Bozkurt, A.; Karadedeli, B. *React. Funct. Polym.* **2007**, *67*, 348–354.

25. Brus, C.; Petersen, H.; Aigner, A.; Czubayko, F.; Kissel, T. *Bioconjugate Chem.* **2004**, *15*, 677-684.

26. Antonietti, L.; Aymonier, C.; Schlotterbeck, U.; Garamus, V. M.; Maksimova, T.; Richtering, W.; Mecking, S. *Macromolecules* **2005**, *38*, 5914-5920.

27. Wang, P.; Meng, K.; Cheng, H.; Hong, S.; Hao, J.; Han, C. C.; Haeger, H. *Polymer* **2009**, *50*, 2154-2160.

28. Yang, Z.; Coutinho, D. H.; Yang, D.-J.; Balkus Jr. K. J.; Ferraris, J. P. *J. Membr. Sci.* **2008**, *313*, 91–96.

29. Krälmer, M.; Pèrignon, N.; Haag, R.; Marty, J.; Thomann, R.; Viguerie, N. L.; Mingotaud, C. *Macromolecules* **2005**, *38*, 8308-8315.

30. Appelhans, D.; Komber, H.; Quadir, M. A.; Richter, S.; Schwarz, S.; Vlist, J.; Aigner, A.; Müller, M.; Loos, K.; Seidel, J. et al. *Biomacromolecules* **2009**, *10*, 1114-1124.

31. Klug, H. P.; Alexander, L. E. *X-Ray diffraction procedures for polycrystalline and amorphous materials*; **1954** John Wiley & Son, Inc: New York.

32. Mitchell, G. R.; Lovell, R.; Windle, A. H. *Polymer* **1980**, *21*, 989-991.

33. Murthy, N. S.; Minor, H. *Polymer* **1990**, *31*, 996-1002.

34. Jithunsa, M.; Tashiro, K.; Nunes, S. P.; Chirachanchai, S. *Polym. Degrad. Stabil.* **2008**, *93*, 1389–1395.

35. Ding, L. *Polymer* **1997**, *38*, 4267-4273.

36. Lee, S.-Y.; Scharfenberger, G.; Meyer, W. H.; Wegner, G. *J. Power Sources* **2006**, *163*, 27–33.

37. He, R.; Li, Q.; Xiao, G.; Bjerrum, N. J. *J. Membr. Sci.* **2003**, *226*, 169–184.